Journal of Power Sources 520 (2022) 230846

Contents lists available at ScienceDirect

Journal of Power Sources

journal homepage: www.elsevier.com/locate/jpowsour

Short thermal treatment of carbon felts for copper-based redox flow batteries

L. Faggiano [a], G. Lacarbonara [a], W.D. Badenhorst [b], L. Murtomäki [b], L. Sanz [c], C. Arbizzani [a,*]

[a] Alma Mater Studiorum - University of Bologna, Dept. of Chemistry "Giacomo Ciamician", Via F. Selmi 2, 40126, Bologna, Italy
[b] Department of Chemistry and Materials Science, Aalto University, PO Box 16100, 00076, Aalto, Finland
[c] Nvision System & Technologies S.L, Avenida Barcelona 105 (Ed. IG Nova Tecnoespai), Igualada, 08700, Barcelona, Spain

HIGHLIGHTS

- Different carbon felts are investigated for an all-Cu redox flow cell.
- Thermal treatment duration is tailored for cost-performance balancing.
- Short thermal treatment increases the electrochemical activity for Cu(I)/Cu(II).
- Surface C═O groups assist redox reaction by non-covalent interaction.

ARTICLE INFO

Keywords:
Carbon felt
Copper redox flow batteries
CuRFB
RFB

ABSTRACT

Carbon felts are often used as electrode materials for various redox flow batteries (RFBs), and for optimal performance it is often required for them to be subjected to extended thermal treatment processes (25–30 h). However, the Cu(II)/Cu(I) redox couple employed in the copper RFB, at the positive electrode is significantly different when compared to the vanadium alternative. For this reason, the effect and duration of thermal treatment of the carbon felt on the performance of the copper-based RFB has to be determined. Both polyacrylonitrile and rayon carbon felts were subjected to thermal treatment for 6 and 25 h at 400 °C. The treated carbon felts were subsequently analysed using thermogravimetric analysis, resistivity determination, scanning electron microscopy, X-ray photoelectron spectroscopy, and Raman spectroscopy. Additionally, the effect of the thermal treatment was also determined using electrochemical testing and in a redox flow cell.

1. Introduction

Redox flow batteries (RFBs) are currently receiving major attention for storing energy from renewable energy sources, as they are considered one of the most appealing solutions to reduce CO_2 emissions and meet growing energy demand in the electricity sector globally. Renewable energy sources require stationary large-size energy storage systems to balance out fluctuations in energy generation and demand. RFBs are suitable systems for this task, able to provide and store large amounts of energy at relatively low cost with long operational lifetime and high efficiencies. RFBs are also interesting since energy and power are decoupled, which allows to tailor them according to any specific application requiring stationary storage. RFBs working with aqueous electrolytes are attractive for its increased safety compared to Li-ion, a key parameter for large-size systems and for household energy storage solutions. The aqueous vanadium RFB (VRFB) is one of the most studied RFB systems, however, the VRFB system suffers from material scarcity and high cost, the latter also due to the need for perfluorinated membranes for electrolyte separation. Various RFBs with other chemistries, such as zinc bromine and iron chromium in aqueous media as well as a wide variety of systems based in organic electrolytes, have been developed and are being employed worldwide [1–6]. Among RFBs operating in aqueous media, several zinc-based chemistries have been studied for flow or hybrid batteries. The most successful of these is the zinc-bromine RFB, which shows a high standard cell voltage (1.85 V) and theoretical specific energy around 440 Wh kg^{-1}. However, the commercial systems generally present specific energy of 60–85 Wh kg^{-1} and is only able to sustain low current densities (tens of mA cm^{-2}) [6].

* Corresponding author.
E-mail address: catia.arbizzani@unibo.it (C. Arbizzani).

https://doi.org/10.1016/j.jpowsour.2021.230846
Received 18 August 2021; Received in revised form 6 November 2021; Accepted 24 November 2021
Available online 8 December 2021

Also, evolution of the classical VRFB such as vanadium-bromine redox flow battery and vanadium–oxygen redox flow battery have been proposed. The former employing vanadium bromide electrolytes, solves the cross-contamination process and allows to increase the vanadium concentration in solution at lower operating temperature. One remaining downside, however, is the emission of toxic bromine vapours that must be reduced or effectively controlled [7]. The latter consists of a VRFB with the positive half-cell replaced with an air electrode. The benefits of increased energy density, reduced quantity of vanadium required, and the limited risk of V(V) precipitation are offset by the swelling stability of the membrane electrode assembly and consequent catalyst layer dissolution [8].

Hruska and Savinell in 1981 [9] proposed the electrochemistry of the all-iron redox flow battery (FeRFB) using the three oxidation state of iron Fe(0)-Fe(II)–Fe(III), which shows a voltage of 1.23 V at 50% state of charge (SoC) taking advantage of non-toxic, low cost and abundant materials. FeRFB shows average power density around 20 mW cm^{-2} and a theoretical energy density of 76 Wh L^{-1} (that practically decreases to ca. 12 Wh L^{-1}) [10].

In contrast to VRFB systems, the exploitation of the copper chemistry in an RFB environment can effectively meet sustainability requirements while operating at relatively lower costs. Copper is a low-cost and abundant element with a well-consolidated value chain in Europe, from extraction to recycling. The copper redox couples have been widely considered for RFB applications and a number of studies have been carried out in organic solvents [11,12], ionic liquids [13], deep eutectic solvents [14] and aqueous solvents [15–19].

The CuRFB system takes advantage of the three stable oxidation states of copper Cu(0)-Cu(I)–Cu(II) in which the cuprous species are transformed in cupric species in the positive half-cell and electrochemically deposited as copper on the negative electrode. Reactions (1) and (2) display the simplified processes occurring at the electrodes, with their standard reduction potentials.

$$\text{Positive half-cell reaction}$$
$$Cu^{+} \underset{\text{Discharge}}{\overset{\text{Charge}}{\rightleftharpoons}} Cu^{2+} + e^{-} \quad E^{0} = 0.158 \text{ V vs SHE} \tag{1}$$

$$\text{Negative half-cell reaction}$$
$$Cu^{+} + e^{-} \underset{\text{Discharge}}{\overset{\text{Charge}}{\rightleftharpoons}} Cu^{0} \quad E^{0} = 0.522 \text{ V vs SHE} \tag{2}$$

However, in chloride-rich media copper cations form chloro-complexes [15] with E^0 shifted according to their increased stability as shown in reactions (3) and (4) [20], and the open circuit voltage (OCV) of the cell can reach 0.65 V at 100% SoC [18].

$$\text{Positive half-cell reaction}$$
$$CuCl_{y}^{1-y} \underset{\text{Discharge}}{\overset{\text{Charge}}{\rightleftharpoons}} CuCl_{x}^{2-x} + \left(x - y\right)Cl^{-} + e^{-} \tag{3}$$

$$\text{Negative half-cell reaction}$$
$$CuCl_{y}^{1-y} + e^{-} \underset{\text{Discharge}}{\overset{\text{Charge}}{\rightleftharpoons}} Cu^{0} + yCl^{-} \tag{4}$$
$$\text{with } 0 \le x \le 4, \quad 0 \le y \le 3$$

Despite the cell voltage being lower than that of VRFBs, an all copper RFB (CuRFB) can provide comparable energy at a lower cost to the VRFB. In commercial VRFB applications, the concentration of V ranges from 1.0 to 1.6 M, given the major complications associated to the precipitation of V^{5+}, which requires a strict temperature control, whereas the higher viable concentration of copper complexes in chloride media can reach 2.5 M. Moreover, copper electrolytes are fully recyclable and can be reused in other applications, as electrolytes in electrowinning industries or as copper etchants for manufacturing printed circuit boards in the electronics industry. To increase the competitiveness of the CuRFB respect to the already established VRFB technology, the various components of the CuRFB should be optimized and validated for long term usage. Stable electrolytes with high concentration of active species, high conductivity, low density and viscosity are required, as well as a mechanically stable separator to limit the unwanted species crossover while maintaining a good ionic permeability. Last but not least, the electrodes should display low resistivity and high surface area and provide a good electron transfer with the electroactive species. Taking a closer look at the system described in Ref. [19], the CuRFB is a hybrid system in which the copper is plated and stripped from the negative electrode while the Cu(II)/Cu(I) redox couple reacts at the positive electrode. Recent developments investigated a bromide supported electrolyte for use in a CuRFB. Despite the higher OCV with respect to chloride supported electrolyte, toxic bromine evolution can occur in case of failures [19].

The present study is focused on the reaction occurring at the positive electrode. Usually, the positive electrode in RFBs is a carbon felt. Hoyt et al. proved the possible employment of carbon felt also for copper plating in a hybrid Cu–Fe cell reaching high plating density (up to 560 mAh cm^{-2}) but with failure problem due to the deposit growth close to the membrane [21]. Several studies have been performed to modify the electrode material in order to improve the redox processes. While the problems related to mass transfer can be easily adjusted by applying suitable flow rates, the issues related to the kinetics of the reaction can be solved only by improving the charge transfer between the surface of the electrode and the active species in solution. In addition, also the ohmic losses due to the electrolyte properties and to the contact resistance, including the electric resistance of the electrode, strongly affect the cell performance. It is evident that a holistic approach to improve the electrolyte properties (concentration of the active species, density, and viscosity), as well as the bulk and interfacial electrode properties is necessary. For VRFBs, chemical, and electrochemical treatments have been suggested for altering the morphology and the chemical composition of the electrode surface [22–26], resulting in improved electrode kinetics. Chemical modification with Bi nanosphere, thanks to strong interfacial Bi–C bonding, improve the mechanical properties of the electrodes under flow rates and catalyze the negative vanadium redox reactions with appreciable activity [23]. Also, chemical modification followed by a thermal enrichment of heteroatoms (e.g. oxygen and nitrogen) to obtain a multiscale-pore-network structured carbon felt was carried out by Wu et al. [24] showing improved properties with respect to pristine carbon felt. Zhou et al. [25] proposed a nano porous structuring of the felt achieving excellent long-term stability up to 2000 cycles. The electrochemical treatments of carbon felts in H_2SO_4 gave very good results in terms of cell performance, with an increase of coulombic, energy and voltage efficiency [26]. Thermal treatments have been demonstrated be effective in producing surface modification of carbon felt, resulting in improved electrochemical performance [27–30]. While chemical and electrochemical methods have their advantages, they are limited in their practical application where low cost materials and process are required, thus thermal treatment are more appropriate for upscale electrode production.

The results of thermal treatment of carbon felt electrodes are reported in this paper and discussed in relation to the use of these materials in CuRFB. Indeed, even if the positive effects of thermal treatments on vanadium reaction are well known [28], there is a lack of information in literature about the effects of the surface treatment of carbon felt on a different chemistry, where copper chloro-complexes dominate the electrochemical processes.

2. Experimental section

The carbon felts (CFs) under study are based on polyacrylonitrile (Ceramaterials, 1/8″) and rayon (Ceramaterials, 1/8”). CFs were used as received (CF_R, CF_P), where R and P stay for rayon and polyacrylonitrile, and thermally treated in air at 400 °C for 6 h and 25 h (CF_R_6h, CF_P_6h and CF_P_25h) by using a ZE muffle furnace (Zetalab). Due to high mass loss values after initial treatment the CF_R was

only treated for a maximum of 6 h.

The pristine and thermally treated CFs were investigated by scanning electron microscopy (SEM), Fourier-transform infrared spectroscopy experiments (FTIR), X-ray photoelectron spectroscopy (XPS), Raman spectroscopy, thermogravimetric analysis (TGA) and cyclic voltammetry (CV). The electrical resistivity of felts was evaluated in two-probe measurement at different compression. Samples with area of 1.5 cm^2 were compressed with different calibration weight. The resistance values were evaluated using Ohms law recording the voltage under a current applied of 10 mA. A scheme of the apparatus is reported in Fig. S1 in the supplementary information. The current was applied with a AMEL 2053 potentiostat and the voltage was recorded with HP 3478A multimeter.

SEM images were collected by a Zeiss EVO 50 microscope and Raman spectroscopy by a microscope RENISHAW Mod INVIA with an Argon ion Laser ($\lambda = 514$ nm, 5 scan, 20s, resolution 1-2 cm^{-1}, 50x).

XPS studies were performed on CF_P samples using a Specs EnviroESCA instrument equipped with an AlKα excitation source ($h\nu$ = 1486.7 eV). Survey spectra were collected at an operating pressure of *ca.* 10-6 mbar in the binding energy (BE) range between 0 and 1460 eV, acquiring data at 100 eV of pass energy, every 1.0 eV•$step^{-1}$, and at 0.1 s•$step^{-1}$. High resolution scans were collected at 40 eV of pass energy, 0.1 eV•$step^{-1}$, and at 0.5 s•$step^{-1}$. XPS curves (BE uncertainty = ± 0.2 eV) were fitted by means of the Keystone software provided by Specs and applying a Shirley-type background function [31]. The shift in terms of binding energy was corrected assigning a value of 284.1/284.4 eV to the C1s peak attributed to carbon sp2-type [27,32,33]. Atomic percentages (at. %) quantification is obtained using the sensitivity factors of integrated peak areas supplied by Specs.

TGA was performed by a TA Instrument Q50 in different conditions: a ramp from 10 °C min^{-1} up to 650 °C, or from 10 °C min^{-1} up to 400 °C and thermal conditioning at 400 °C for 6 h. TGA were carried out with Ar both as the purge gas at 60 mL min^{-1} and the sample gas (O_20) at 40 mL min^{-1}; Ar at 60 mL min^{-1} (purge) and O_2 (O_240) at 40 mL min^{-1} (sample); Ar at 80 mL min^{-1} (purge) and O_2 as sample gas (O_220) at 20 mL min^{-1} (sample). Some CF_R samples were dried at 60 °C for 20 h before TGA analysis.

FTIR spectra were collected by using a Bruker Alpha by accumulating a minimum of 24 scans per sample with a resolution of 5 cm^{-1}. The CF material was ground with KBr in the weight ratio of 1:200 and the mix of powders was pressed at 6 ton for 2.5 min. The spectra are reported in Fig. S2.

CV experiments were carried out in a three-electrode conventional cell (Lithium Battery Cell Gamry) with a graphite rod (6 mm diameter, Gamry) as counter electrode and a saturated calomel electrode (SCE, AMEL, 303/SCG/6J) as reference electrode at 40 °C by using a Voltalab PGZ301 (Radiometer Copenhagen, Denmark). The working electrode was a carbon felt (CF, 0.15 cm^2) fixed in the electrode holder by the screw cap and a silicon gasket, an electric contact assured via a Ti current collector. The electrode holder scheme is shown in Fig. S3. The solution (25 mL) was degassed with Ar before starting the measurements. The CF, fixed in the silicon gasket, were kept in the diluted solutions over night before assembly in the holder, and for 30 min in concentrated solution. A glassy carbon electrode (GC, 0.11 cm^2) was used as working electrode for comparison.

The electrochemical tests were carried out in the following solutions: (a) 5 mM ferrocene methanol (FcMe) in phosphate buffer solution (PBS) to evaluate the effective active area of CFs, (b) a diluted 5 mM $CuCl_2$ in 1 M HCl solution to evaluate the electrochemical response of CFs and (c) a concentrated 2 M $CuCl_2$ in 6 M HCl to simulate the RFB conditions. The conductivity of the solutions was measured by a four-point conductivity cell (Radiometer analytical CDC86IT, Copenhagen, Denmark) by impedance spectroscopy (EIS) using a BioLogic VSP multichannel potentiostat/galvanostat/FRA. The EIS was performed with a 100 kHz–10 kHz frequency range and 5 mV AC perturbation, acquiring 10 points.

The in-house made redox flow cell (RFC) consisted of the CF_P_6h positive electrode and a graphite bipolar plate (Sigracell FR-10) as substrate for deposition of copper separated by a commercial separator (Daramic-CL) and the electrolyte solution (2 M CuCl – 1 M $CaCl_2$ – 6 M HCl) corresponding to 0% SoC. The RFC and the cell scheme are shown in Fig. S4.

Galvanostatic charge/discharge tests were performed with a flow rate of 60 mL min^{-1} (referred to pure water), by using a peristaltic pump (model 323, Watson Marlow) with Marprene tubes at 60 rpm. The tanks with 50 mL electrolyte each were maintained in a thermostatic bath (Julabo Labortechnik GmbH) at 60 °C and the cell temperature was kept constant with two electric heating pads applied to the aluminium end plates. The galvanostatic test consisted of 5 cycles at different current density (20 mA cm^{-2}, 30 mA cm^{-2}, 40 mA cm^{-2} and 50 mA cm^{-2}), performed in continuous mode and maintaining the same solution till the end, setting cut off voltages of 0 V and 0.9 V. The CF_P_6h electrode and the Daramic-CL separators were kept in 6 M HCl before assembly in RFC. The electrolytes were circulated for 30 min for pre-conditioning the system before testing was commenced.

The values of coulombic efficiency are calculated by the ratio between the supplied charge (Q_{dis}) and the stored charge (Q_{ch}):

$$CE\ (\%) = \frac{Q_{dis}}{Q_{ch}} * 100\%$$

The values of voltage efficiency are calculated by the ratio between the average voltage during discharge mode (V_{dis}) and average voltage during charge mode (V_{ch}):

$$VE\ (\%) = \frac{V_{dis}}{V_{ch}} * 100\%$$

The chemicals PBS (Oxoid itd, tablets), ferrocene methanol (FM, 97%, Sigma Aldrich), $CuCl_2$ (99.99 + %, Sigma Aldrich), CuCl (≥99.995% trace metal basis, Sigma Aldrich, HCl (37%, Sigma-Aldrich), $CaCl_2$ (≥99%, ACS reagent, Sigma Aldrich) were used as received. MilliQ water (18 MΩ cm) was used for the solutions that were deaerated with Ar for 10 min.

3. Results and discussion

3.1. Physicochemical characterization

3.1.1. TGA analysis

To evaluate the appropriate temperature for the treatment of the CFs, TGA analyses have been conducted to study the thermal stability of the carbon felt materials. Fig. 1a shows the thermal degradation of the two pristine CFs in the presence of O_2 (O_240). The response of the two samples to the oxidative atmosphere differs, and it can be ascribed to different precursor materials and manufacturing techniques employed for either felt [30]. For its polysaccharide precursors, rayon has a higher capacity to adsorb water content in air atmosphere compared to polyacrylonitrile and this behaviour is highlighted by the higher mass loss at low temperature (<100 °C) of CF_R ascribed to water evaporation. In rayon-based felt, a continuous mass loss is observed by increasing of the temperature due to superficial degradation of the material. The complete degradation of the felts structure occurs over when the temperature exceeds 420 °C, where the fibre chains are entirely decomposed. On the other hand, the initial degradation of CF_P sample starts when exceeding 500 °C with a loss of about 20% of weight at 650 °C. The CF_R sample analysed in Ar atmosphere (blue line) was not dried before TGA. During the TGA the CF_R sample displayed 12% initial mass loss, caused by evaporation of water content, with thermal degradation started when temperatures above 470 °C was achieved. Fig. 1b displays the behaviour of CF_R samples in conditions that mimic the thermal treatment in air. The O_2 flow over sample was decreased to 20 mL min^{-1} (O_220), and the isothermal test at 400 °C was performed after a short ramp that simulates the increasing temperature of the muffle furnace up to reaching

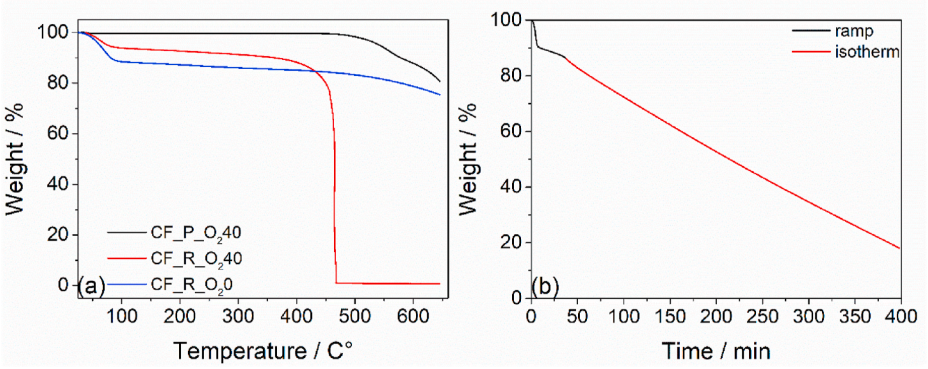

Fig. 1. Thermogravimetric analysis (10 °C min^{-1}) of pristine CF materials (a) CF_R (red) and CF_P (black) in presence of O_2 ($O_2$40) and CF_R (blue) in Argon ($O_2$0) (b) CF_R in presence of O_2 ($O_2$20) in isothermal condition at 400 °C (red) after a short ramp (ca. 40 min, 10 °C min^{-1}) up to 400 °C (black). (For interpretation of the references to colour in this figure legend, the reader is referred to the Web version of this article.)

400 °C. During this temperature ramping a continuous mass loss is evident: 14% weight is lost during the heating ramp in the first 40 min, and 68% in the 6 h at 400 °C. The mass losses during TGA are higher than those found after thermal treatment in the muffle furnace (>50%). The behaviour can be attributed to the continuous flow of O_2 on the sample during TGA, removing degraded fibres and exposing new fibres to the oxidation process. This flow and removal of degraded fibres does not occur in the static conditions inside the muffle furnace. The high weight loss of CF_R indicates the lower thermal stability of the material with respect to CF_P. Hence, the CF_R exposure at high temperature was limited to 6 h, to prevent excessive degradation of the CF_R carbon felt.

3.1.2. SEM imaging

The morphologies of the different CFs are shown in Fig. 2. All samples show randomly distributed fibres, with the morphology depending on the starting material and manufacturing route employed [21]. The CF_R consists of bundles of smooth fibres in contrast to polyacrylonitrile-based felt consisting of single fibres with surface veining. The diameter of CF_R bundles and CF_P fibres were similar (ca. 20 μm) while the diameter of the individual fibres of the CF_R felt are nearly a few μm across. The two different precursors showed dissimilar responses to the thermal treatment at 400 °C, as expected through TGA analysis. The CF_R samples degradation largely depends on the duration of thermal treatment as the degradation process is initiated near 400 °C. In Fig. 2b, yellow arrows highlight the presence of cavities on the surface of CF_R fibres giving an irregular shape to the edges. On the contrary, CF_P fibers in Fig. 2d and e do not show other modifications of the morphology other than the observed increase of roughness.

3.1.3. X-ray photoelectron spectroscopy

In Fig. S5 the full survey XPS spectra of CF_P, CF_P_6h, and CF_P_25h shows the characteristic peaks of C1s and O1s at 284 eV and 532 eV, respectively. The integrals of these signals indicate the atomic content (Table 1) is influenced by the thermal treatment duration. In CF_P, the C1s band is the main contribution in the survey XPS spectra. Increasing the treatment duration, the signal relative at the O1s increases indicating a higher presence of oxygen groups in the material.

The XPS high resolution of C1s exhibit contributions of C═C carbon at 284.1 eV, C–H at 284.9 eV, C–O-R at 286.0 eV, and C═O at 288.2 eV [27,32]. The effect of the thermal treatment (Fig. 3b and 3c) reflects on the higher amount of C–H and C–O groups with respect to the C═C presented in CF_P (Fig. 3a). The high-resolution spectrum of the O 1s region shows two peaks for all the samples with binding energy at 533.5 eV and 531.0 eV, corresponding to the C–O and C═O functional groups, respectively. However, the two different contributions change significantly with the thermal treatment. In contrast to the CF_P (Fig. 3d), the CF_P_6h significantly increases oxygen functional groups with the C═O that increases more respect to the C–O (Fig. 3e). Proceeding in the thermal treatment (CF_P_25h in Fig. 3f), the oxygen content continues to grow with the increment of C–O functionalities at the expense of carbonyl functional groups. The percentages of the different C–C and C–O groups with the corresponding binding energy is given in Table 2.

3.1.4. Raman spectroscopy

The carbonaceous structure of pristine and thermally treated CFs was investigated using Raman analysis. The different hybridization of carbon atoms and the distribution of disorder are considered to define the carbon materials' structure. An ordered structure, like graphene, is highlighted by the presence of the G band that is related to the vibration of sp^2 carbon atoms. On the other hand, defects or heteroatoms characterize the D band [34,35].

The deconvolution of the acquired spectra has been done in the range of wavenumber between 1000 and 2000 cm^{-1} and involves 4 Lorentzian and 1 Gaussian functions, as shows in Fig. 4. The I_{D1}/I_G and $I_{D1}/I_G + I_{D1}$ (D-to-G ratios) values were calculated using the integrated intensity, the results of which are reported in Table 3. In the case of polyacrylonitrile-based samples, the D-to-G ratios for pristine and 6h-thermal treated electrodes are moderately similar, and only slight variations occur after 25h-treatment of treatment. In PAN-based felts, the full width at half maximum (FWHM) of D-band is higher than that of G-band, and this does not vary with thermal treatment. It suggests that there are no significant changes in the structural organization of the felt. In the case of the rayon-based felt, the pristine and 6h-treated samples show a higher difference of the D-to-G ratios. In the pristine sample, the contribution of the D band is lower than that of the G band, suggesting a high content of ordered atoms. Indeed, the FWHM-G is higher than of FWHM-D. On the other hand, with the treatment, the FHWM-D increases by three times, indicating a more extensive oxidation of the surface.

3.1.5. Resistivity measurements

The electrical resistivity of the carbon felts was evaluated under varying load and compression values. As previously reported [36,37], the resistivity of these materials decreases linearly with compression for the first 20% to reach an asymptotic value. At low compression, contact points are scarce and the characteristic value of the material can be taken by increasing the compression to over 20%.

Fig. 5 shows that CF_R has the maximum resistivity (1.60 Ω cm) among the samples tested, reaching the highest compression of 40% with a load of 315 g cm^{-2}. Additionally, after thermal treatment, sample CF_R became brittle and difficult to handle and was thus not tested. Alternatively, the PAN-based felts show the lowest resistivity, 0.17–0.14 Ω cm in the asymptotic part of the curve. The CF_P_6h and pristine CF_P felts show similar compression, exhibiting ca. a 20% of thickness variation with a load of 315 g cm^{-2}. On the contrary, CF_P_25h

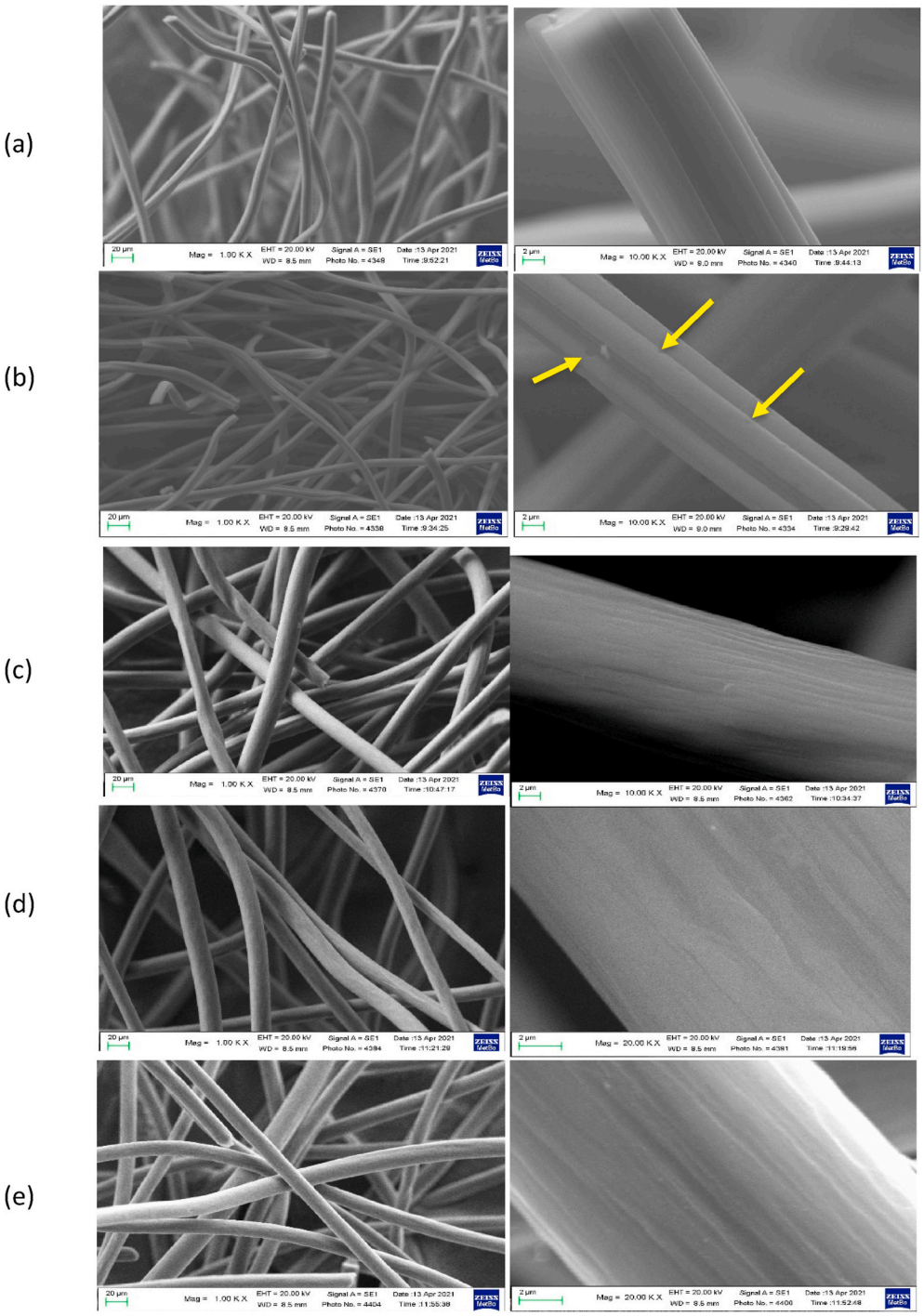

Fig. 2. SEM images of thermal treated samples: (a) CF_R; (b) CF_R_6h; (c) CF_P; (d) CF_P_6h and (e) CF_P_25h

Table 1
Atomic content of polyacrylonitrile-based carbon felts from integrals of C1s and O1s signals.

Sample	C1s	O1s
CF_P	95.6%	3.8%
CF_P_6h	90.7%	9.0%
CF_P_25h	81.1%	18.8%

shows 40% compression with the same load. The highest stiffness of the CF_P_6h ensures a better performance in the RFB cell in which the materials are under pressure generated from the hydraulic system.

3.2. Electrochemical characterization

3.2.1. Cyclic voltammetry in conventional three-electrode cell

Electrochemical tests were performed using a three-electrode cell. The samples were immersed in the testing solution before assembly in an electrode holder as described. Pristine CF_R samples showed higher wettability compared to the PAN-felts, with the higher hydrophilicity of the rayon carbon felt leading to the presence of polar groups in the carbon structure [21]. However, thermal treatment causes the rayon-based felt to become brittle, leading to fibres becoming lost/broken during handling and immersion in the solution. This is also the reason why attempts to perform the CV tests as described below for

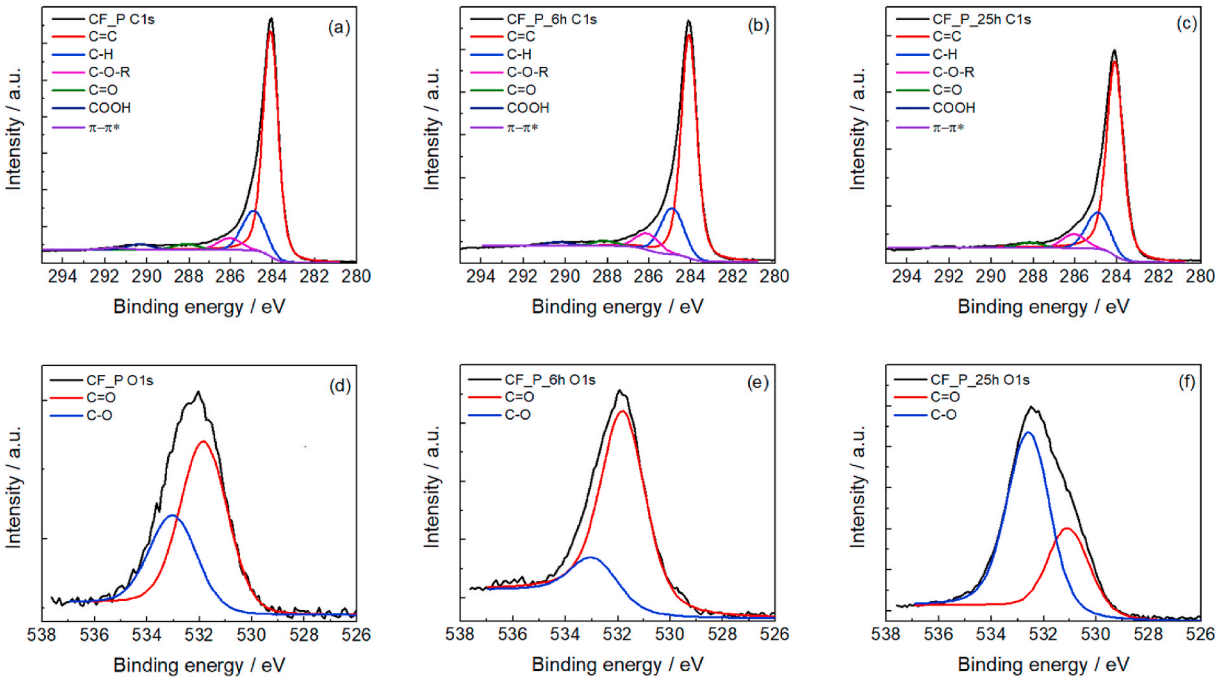

Fig. 3. High-resolution XPS spectra of C1s region (a–c) and O1s region (d–f) fitting of the polyacrylonitrile-based carbon felts: CF_P (a, d), CF_P_6h (b, e) and CF_P_25h (c, f).

Table 2
Speciation of C1s and O1s energetic regions.

O1s	C=O	C–O				
CF_P	65.5%	34.5%				
CF_P_6h	84.3%	15.7%				
CF_P_25h	33.7%	66.3%				
Binding Energy (eV)	533.0	531.8				
C1s	C=C	C–C	C–O-R	C=O	COOH	π →π*
CF_P	72.4%	16.9%	5.0%	2.5%	2.3%	0.9%
CF_P_6h	71.2%	18.6%	6.6%	2.0%	1.6%	0%
CF_P_25h	74.5%	16.6%	6.3%	2.4%	1.7%	0.2%
Binding Energy (eV)	284.1	284.9	286.0	288.2	290.4	291.5

the rayon-based felts failed. In contrast, the thermal treatment on CF_P samples improved the electrode wettability by increasing the content of oxidized groups on the surface without affecting the mechanical integrity of the material.

The polyacrylonitrile-based felts were fixed into a circular gasket and tested in 5 mM FcMe - PBS to evaluate their effective area (EA_{CF}) compared to that of a GC electrode. The redox couple $FcMe^+$/FcMe was selected because of its redox potential (0.4 V vs SHE [38]) is in the same range of the potential of the Cu(I)/Cu(II) couple. The CVs at 10 mV s^{-1} in Fig. 6a and at 100 mV s^{-1} in Fig. 6b reveal the different areas of the CFs and of the GC electrode. EA_{CF} was calculated by the ratio of the anodic peak current density of the CFs and of the GC. All the felts, once well wet, reach a similar current showing unvaried reactivity after the thermal treatment. The carbon felt areas are at least 30 times higher than that of GC, with the resulting areas being summarized in Table 4 The peak separation (ΔE) for felt electrodes is smaller than 0.057 V indicating a good reversibility of the process on carbon felt surface. Accordingly, the i_{pc}/i_{pa} ratio is close to 1. For all the samples the $(E_+ + E_-)/2$ is around 0.185 V vs SCE.

Tests in diluted solution of $CuCl_2$ were carried out using the same assembly and procedure previously described to evaluate the effect of a different chemistry (Cu(II)/Cu(I) vs. $FcMe^+$/FcMe). The CVs of the polyacrilonitrile-based felts in 5 mM $CuCl_2$ – 1 M HCl and in 2 M $CuCl_2$ – 6 M HCl are shown in Fig. 7. The pristine CF_P shows a well-defined

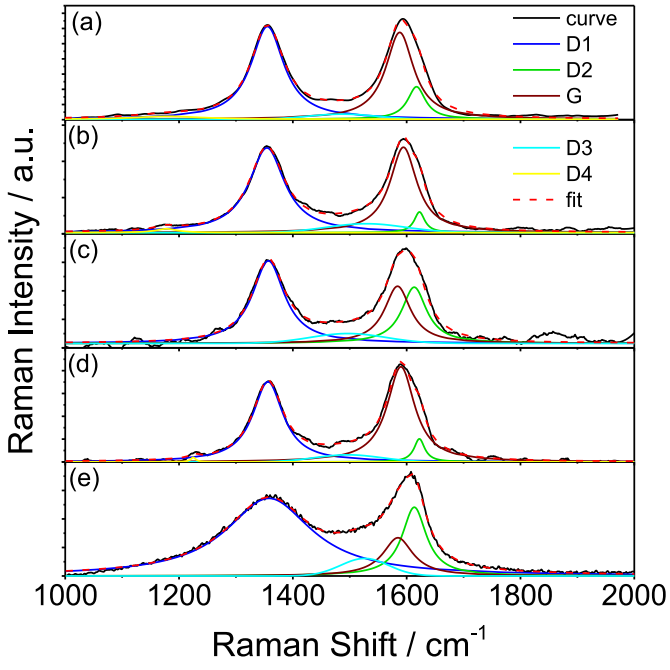

Fig. 4. Raman spectra of carbon materials. a) CF_P; b) CF_P_6h; c) CF_P_25h; d) CF_R; e) CF_R_6h.

oxidation peak and a flattened reduction peak at low scan rate (Fig. 7a). The flattened peak can be attributed to the slower kinetics of the electron transfer process due to the higher resistivity of pristine CF_P compared with the thermal treated CF_P_6h and CF_P_25h. The increasing in scan rate exacerbates this feature (Fig. 7b). The reduction process needs higher overpotential to occur and the shape of the current profile, almost constant at potential lower than 0.2 V, indicates a kinetically limited behaviour. After the thermal treatment, the CVs becomes more reversible, even with only 6h treatment.

In Table 5 the electrochemical parameters obtained from the CVs at

Table 3
Calculated parameters of deconvoluted function of Raman spectra of the different samples.

Sample	Area	Centre (cm^{-1})	FWHM	I_{D1}/I_G	$I_{D1}/I_G + I_{D1}$
CF_P	$64.8•10^3$ (D1)	1355 (D1)	70 (D1)	1.25	0.55
	$51.5•10^3$ (G)	1587 (G)	60 (G)		
CF_P_6h	$26.4•10^3$ (D1)	1354 (D1)	76 (D1)	1.28	0.56
	$20.5•10^3$ (G)	1594 (G)	58 (G)		
CF_P_25h	$8.9•10^3$ (D1)	1357 (D1)	66 (D1)	1.75	0.63
	$5.1•10^3$ (G)	1584 (G)	55 (G)		
CF_R	$17.1•10^3$ (D1)	1356 (D1)	59 (D1)	0.92	0.47
	$18.5•10^3$ (G)	1590 (G)	65 (G)		
CF_R_6h	$342.3•10^3$ (D1)	1358 (D1)	183 (D1)	5.32	0.84
	$64.2•10^3$ (G)	1584 (G)	64 (G)		

10 mV s^{-1} are reported. In all the tested samples, the high ΔE values suggest the quasi-reversibility of the electrochemical processes, and the lowest peak separation is achieved by the CF_P_6h (0.140 V). The i_{pa}/i_{pc} ratio is 2.12 for the pristine felt, which decrease significantly with the thermal treatment and reaches values near 1.

The better performance of CF_P_6h demonstrates that the optimal surface modification is reached after 6 h of thermal treatment to produce a wettable electrode able to exchange electrons with the copper chloro-complexes present in the electrolyte; whereas CFs for vanadium RFB have been demonstrated to require 25–30 h of thermal activation [20].

Fig. 7c displays the CVs of the polyacrylonitrile-based carbon felts in the concentrated solution 2 M $CuCl_2$ with 6 M HCl. While the concentrated electrolyte displays higher conductivity than the diluted one (634 vs. 325 mS cm^{-1} at 40 °C), the higher ionic strength and viscosity affects ion diffusion. In addition, the types of chloro-complex present in the solution and their stability, which affect the potentials of the redox processes, also depends on the ratio Cu:Cl:H_2O [39,40]. The shift of both anodic and cathodic processes to higher and lower potential, respectively, indicates kinetic limitations of the electron transfer. CF_P displays the anodic process peak near 0.9 V, while the cathodic one is close to the copper plating process and cannot be observed. CF_P_6h shows the processes peaks within the potential stability window, although with a ΔE of ca. 0.87 V, and $(E_+ + E_-)/2$ of 0.215 V. In the concentrated electrolyte, the higher viscosity and density of the solution made the voltammetric investigation possible also on CF_R_6h, even if only few cycles could be performed with not separated compartments, which are reported in the supplementary information (Fig. S6). Repeated CVs were also carried out (and reported in Fig. S7), evidencing that no poisoning effects are observed due to the presence of chloride ions.

Summarizing the information from physicochemical and electrochemical characterizations, some aspects of the electrochemical process occurring at the positive electrode of a CuRFB can be compared with the process occurring in VRFB. In VRFB, the oxygen-containing groups act as the electrocatalytic active sites. In fact, in the positive half-cell, the charge and discharge processes at the positive electrode involve the

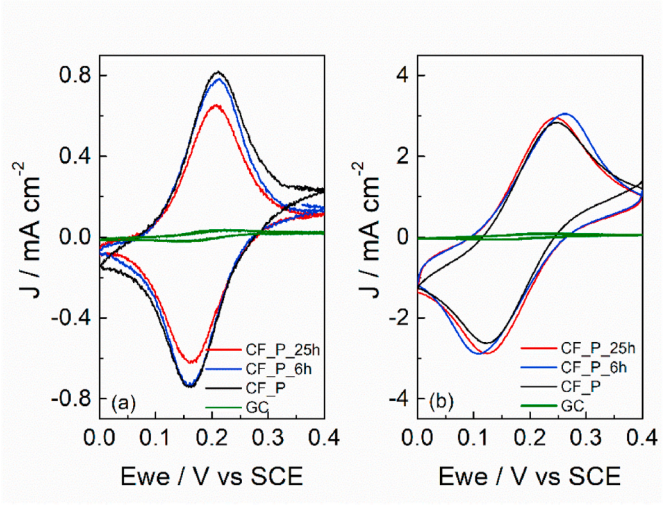

Fig. 6. CVs at 40 °C on GC, pristine, and treated polyacrylonitrile-based carbon felts in 5 mM ferrocene-methanol in PBS solution at (a) 10 mV s^{-1} and (b)100 mV s^{-1}.

Table 4
Summary values of different carbon felts in 5 mM FcMe - PBS at 10 mV s^{-1}

Sample	i_{pa} mA cm^{-2}	A	i_{pc}/i_{pa}	ΔE V vs SCE	$(E_+ + E_-)/2$ V vs SCE
GC	0.020	1	0.95	0.080	0.184
CF_P	0.538	27	1.2	0.048	0.186
CF_P_6h	0.698	35	0.93	0.055	0.185
CF_P_25h	0.556	29	0.97	0.042	0.184

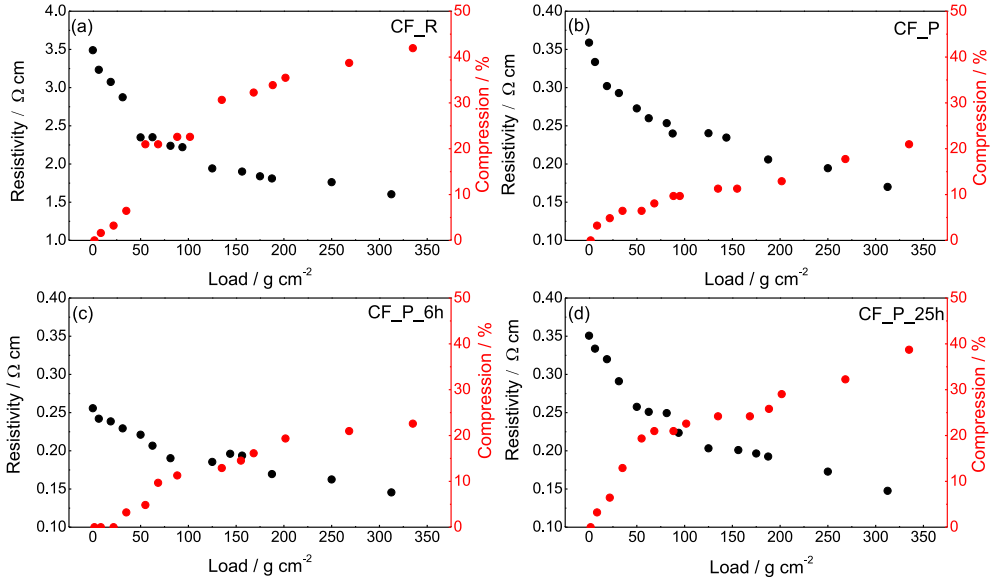

Fig. 5. Electrical resistivity and compression vs applied load for CF_R (a), CF_P (b), CF_P_6h (c), CF_P_25h (d).

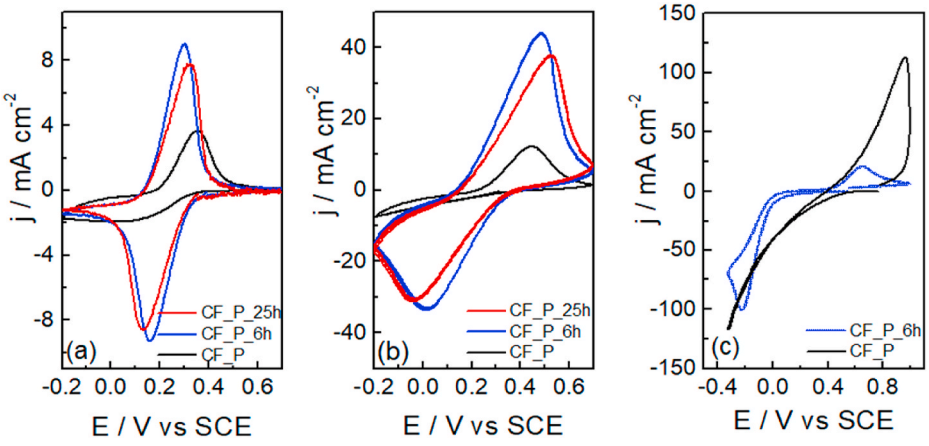

Fig. 7. CVs at 40 °C of pristine, and treated polyacrylonitrile-based carbon felts in 5 mM $CuCl_2$ 1 M HCl solution at (a) 10 mV s^{-1} and (b) 100 mV s^{-1}, and (c) in 2 M $CuCl_2$ – 6 M HCl solution at 10 mV s^{-1}.

Table 5
Electrochemical parameters from CVs at 10 mV s^{-1} of different carbon felts in 5 mM $CuCl_2$ 1 M HCl solution at 40 °C.

Sample	i_{pa}/i_{pc}	ΔE V vs SCE	$(E_+ + E_-)/2$ V vs SCE	OCV V vs SCE
CF_P	2.12	0.252	0.226	0.386
CF_P_6h	1.11	0.140	0.230	0.391
CF_P_25h	1.03	0.190	0.228	0.355

transfer of an oxygen atom, which can be the rate determining step in the overall reaction. So, the availability of oxygen groups on the electrode surface affects the rate of the reaction. The electron transfer from the VO^{2+} to the electrode occurs along with the -C-O-V- bond and transfer of one oxygen atom on the C–O functional group to the VO^{2+}, forming a surface VO_2^+. Hence, a long thermal treatment is necessary for VRFB in order to enrich the carbon surface of -C-O functionalities. In an all-copper redox flow system, the interaction of copper with the electrolyte and the electrode surface is regulated by intermolecular interactions. The presence of C═O groups on the electrode surface can assist the electrochemical reaction coordinating copper cations without covalently bonding the electroactive species to the electrode surface. Moreover, C–O-R end group results sterically hindered (R = aliphatic groups) or protonated (R = H), with an electron-donor effect in acid environment lower than that of C═O functionalities. As proposed in Scheme 1, electroactive species (Cu(I) chlorocomplexes) move from the bulk to the electrode interphase (1), and can be assisted in their further approach to the electrode surface by the Cu–O non-covalent interaction (2). The electron transfer occurs (3) and the produced Cu(II) chlorocomplexes move away from the electrode-electrolyte interphase. Furthermore, the presence of more carbonyl groups than C–O guarantees a better conductivity of CF_P_6h compared to CF_P_25h due to the possible electronic conjugation of double bonds to the extended aromatic coordination of the carbonaceous matrix.

3.2.2. Galvanostatic charge/discharge cycles in redox flow cell

A redox flow cell (RFC) with the CF_P_6h as positive electrode, graphite bipolar plate for the negative process, 2 M CuCl – 1 M $CaCl_2$ – 6 M HCl solutions as the electrolyte and a Daramic-CL porous separator were assembled and tested. Charge-discharge cycles (30 min charge followed by 30 min discharge) between 20 and 50 mA cm^{-2} were carried out to evaluate the electrode behaviour in the RFC (Fig. 8). Starting from 0% SoC the cell can reach only a 10% of charge in 30 min. The voltage profiles at the different current densities are very similar, with the current values mainly affecting the charging process rather than the discharge. Initial OCV values were taken 0.515 V, i.e. the voltage after

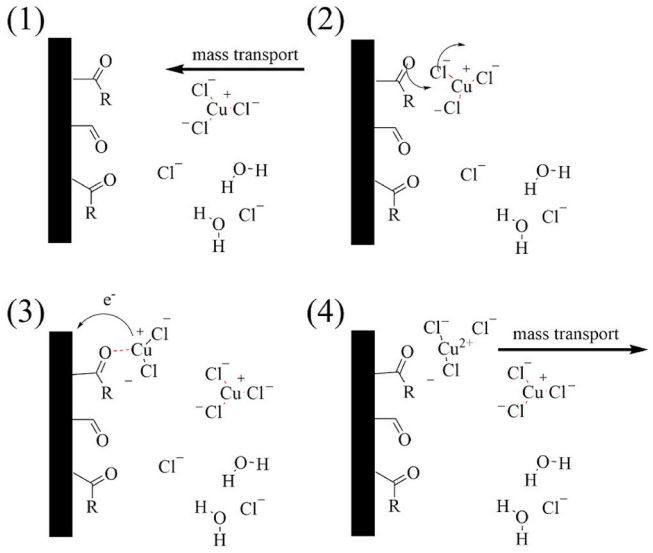

Scheme 1. Proposed mechanism for Cu(I)–Cu(II) redox reaction with C═O functional groups on the electrode surface as high affinity coordinating site. (1) mass transport of the Cu(I) chlorocomplexes at the electrode interphase; (2) interaction of copper with surface C═O groups; (3) electron transfer; (4) mass transport of the Cu(II) chlorocomplexes toward bulk electrolyte.

the first 5 cycles at 20 mA cm^{-2}, and as final value the OCV measured after the 5 cycles at 50 mA cm^{-2} (0.568 V), as can be seen in Table 6. During discharge, the processes of Cu dissolution and Cu(II) reduction shows a low overpotential even at high currents, changing the average discharge voltage from ca. 0.43 V at 20 mA cm^{-2} to 0.38 V at 50 mA cm^{-2}.

The optimization of the plating process at the negative electrode is one of the most critical issues in a hybrid RFB system as it could reduce the electrode overpotential, and further improvement in membrane performance and in the flow management can increase the coulombic efficiency by preventing electrolyte crossover phenomena. Table 6 reports the values of coulombic efficiency (CE) and voltage efficiency (VE) for the average of 5 cycles at each current density. Without any optimizations, the RFC shows a CE of 87% and a VE of 60% at 30 mA cm^{-2}, thus demonstrating the effectiveness of the short thermal treatment of PAN carbon felts.

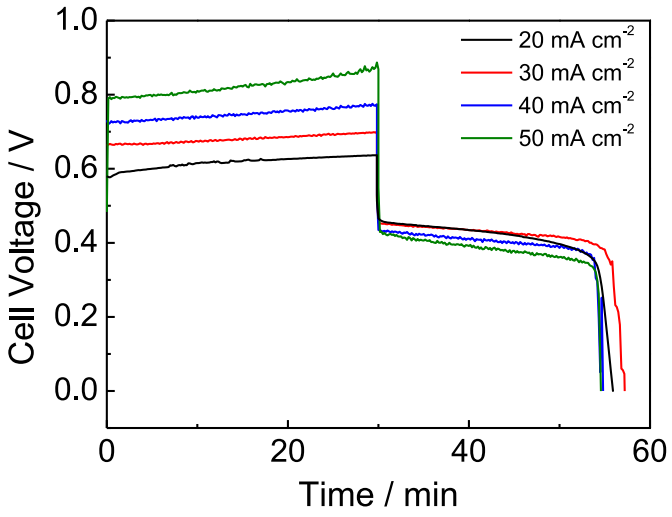

Fig. 8. Voltage profile of the 5th cycle at each current density of the RFC with 30 min charge and 30 min discharge cycles at 60 °C.

Table 6
Open current voltage of the 1st cycle, average values of coulombic efficiency and voltage efficiency of 5 galvanostatic cycles at different current densities with CF_P_6h positive electrode.

Current density mA cm^{-2}	OCV V	CE %	VE %
20	–	79	68
30	0.515	87	60
40	0.526	85	53
50	0.549	83	56

4. Conclusions

The activation of carbon felts to be used as positive electrodes in all-copper RFBs is one of the key issues for achieving good battery performance. In this work, two carbon felts using the polyacrylonitrile and rayon precursors, have been investigated together with thermal activation of these felts. As expected, they needed thermal activation to improve their wettability for the use in aqueous media. However, thermal treatment affects the structural integrity of the two materials, with the rayon-based treated carbon felt becoming very brittle and difficult to handle. On the other hand, polyacrylonitrile-based carbon felt demonstrated an excellent stability and the best electrochemical performance after 6 h of thermal treatment at 400 °C. Differently from CFs for VRFB electrodes, which require longer activation periods due to the reaction at the positive electrode involving covalent bonds with CO surface groups, the CF used in copper RFBs need a shorter activation time because the oxygen groups only assist the reaction by intermolecular interactions. The feasibility of the short heat treatment for polyacrilonitrile-based CF electrodes has been demonstrated also in an RFC configuration. Although the RFC assembly and components were not optimized, an efficiency of 92% (last cycle at 30 mA cm^{-2}) and the ability to sustain currents up to 50 mA cm^{-2} have been proved.

Finally, some considerations on cost and sustainability. The total cost of a cell comprises the cost of materials and material processing and is considered both in terms of cost and energy consumption. A thermal treatment of 6h was proved to be sufficient to improve the electrochemical performance of the electrode, which is an important result towards the scale up of the all-copper RFB, since shortening the thermal treatment of the electrodes positively affects the total cost of cells and stacks, as well as the carbon footprint associated to the manufacturing processes. If the energy used for these processes is not sourced from renewable sources, the shortening of thermal treatments means lower energy consumed and lower carbon dioxide emission, which are key issues for the value chain of CuRFBs.

CRediT authorship contribution statement

L. Faggiano: Conceptualization, Investigation, Validation, Formal analysis, Data curation, Writing – review & editing. **G. Lacarbonara:** Methodology, Formal analysis, Visualization, Writing – review & editing. **W.D. Badenhorst:** Resources, Formal analysis, Writing – review & editing. **L. Murtomäki:** Writing – review & editing, Funding acquisition, Project administration. **L. Sanz:** Writing – review & editing, Funding acquisition, Project administration. **C. Arbizzani:** Conceptualization, Writing – original draft, Writing – review & editing, Funding acquisition, Project administration, Supervision.

Declaration of competing interest

The authors declare that they have no known competing financial interests or personal relationships that could have appeared to influence the work reported in this paper.

Acknowledgments

This work was supported by the European Union within the Horizon 2020 research and innovation programme [CUBER - Copper-Based Flow Battery for Energy storage Renewables Integration H2020 - LC - BAT_2019] under grant agreement No. 875605. All the Project Partners are acknowledged for the fruitful discussion. G.L. acknowledges the Department of Excellence program financed by the Minister of Education, University and Research (MIUR, L. 232 del December 01/12/2016) for the doctoral scholarship. Our deepest gratitude to Prof. V. Di Noto and Dr. G. Pagot (University of Padua) for XPS measurements.

Appendix A. Supplementary data

Supplementary data to this article can be found online at https://doi.org/10.1016/j.jpowsour.2021.230846.

References

[1] M. Skyllas-Kazacos, Flow batteries, in: H. Zhang, X. Li, J. Zhang (Eds.), Redox Flow Batteries, CRC Press, 2017, pp. 327–354, https://doi.org/10.1201/9781315152684-9.
[2] J. Noak, N. Roznyatovskaya, T. Herr, P. Fischer, The chemistry of redox-flow batteries, Angew. Chem. Int. Ed. 54 (2015) 9776–9809, https://doi.org/10.1002/anie.201410823.
[3] R. Ye, D. Henkensmeier, S.J. Yoon, Z. Huang, D.K. Kim, Z. Chang, S. Kim, R. Chen, Redox flow batteries for energy storage: a technology review, J. Electrochem. En. Conv. Stor 15 (1) (2018) 10801, https://doi.org/10.1115/1.4037248.
[4] K. Lourenssen, J. Williams, F. Ahmadpour, R. Clemmer, S. Tasnim, Vanadium redox flow batteries: a comprehensive review, J. Energy Storage 25 (2019) 100844, https://doi.org/10.1016/j.est.2019.100844.
[5] P. Leung, A.A. Shah, L. Sanz, C. Flox, J.R. Morantec, Q. Xu, M.R. Mohamed, C. Ponce de León, F.C. Walsh, Recent developments in organic redox flow batteries: a critical review, J. Power Sources 360 (2017) 243–283, https://doi.org/10.1016/j.jpowsour.2017.05.057.
[6] E. Sánchez-Díez, E. Ventosa, M. Guarnieri, A. Trovò, C. Flox, R. Marcilla, F. Soavi, P. Mazur, E. Aranzabe, R. Ferret, Redox flow batteries: status and perspective towards sustainable stationary energy storage, J. Power Sources 481 (2021) 228804, https://doi.org/10.1016/j.jpowsour.2020.228804.
[7] M. Skyllas-Kazacos, G. Kazacos, G. Poon, H. Verseema, Recent advances with UNSW vanadium-based redox flow batteries, Int. J. Energy Res. 34 (2010) 182–189, https://doi.org/10.1002/er.1658.
[8] P. Alotto, M. Guarnieri, F. Moro, Redox flow batteries for the storage of renewable energy: a review, Renew. Sustain. Energy Rev. 29 (2014) 325–335, https://doi.org/10.1016/j.rser.2013.08.001.
[9] L.W. Hruska, R.F. Savinell, Investigation of factors affecting performance of the iron-redox battery, J. Electrochem. Soc. 128 (1981) 18, https://doi.org/10.1149/1.2127757.
[10] M.C. Tucker, A. Phillips, A.Z. Weber, All-iron redox flow battery tailored for off-grid portable Application, Chem. Sus. Chem. 23 (2015) 3996–4004, https://doi.org/10.1002/cssc.201500845.

[11] B. Kratochvil, K.R. Betty, A secondary battery based on the copper(II)-(I) and (I)-(0) couples in acetonitrile, J. Electrochem. Soc. 121 (1974) 851–854, https://doi.org/10.1149/1.2401935.
[12] Y. Li, J. Sniekers, J. Malaquias, X. Li, S. Schaltin, L. Stappers, K. Binnemans, J. Fransaer, I.F.J. Vankelecom, A non-aqueous all-copper redox flow battery with highly soluble active species, Electrochim. Acta 236 (2017) 116–121, https://doi.org/10.1016/j.electacta.2017.03.039.
[13] D. Lloyd, T. Vainikka, S. Schmachtel, L. Murtomaki, K. Kontturi, Simultaneous characterization of electrode kinetics and electrolyte properties in ionic liquids using a rotating disc electrode, Electrochim. Acta 69 (2012) 139–145, https://doi.org/10.1016/j.electacta.2012.02.104.
[14] D. Lloyd, T. Vainikka, K. Kontturi, The development of an all copper hybrid redox flow battery using deep eutectic solvents, Electrochim. Acta 100 (2013) 18–23, https://doi.org/10.1016/j.electacta.2013.03.130.
[15] L. Sanz, J. Palma, E. García-Quismondo, M. Anderson, The effect of chloride ion complexation on reversibility and redox potential of the Cu(II)/Cu(I) couple for use in redox flow batteries, J. Power Sources 224 (2013) 278–284, https://doi.org/10.1016/j.jpowsour.2012.10.005.
[16] L. Sanz, D. Lloyd, E. Magdalena, J. Palma, M. Anderson, K. Kontturi, Study and characterization of positive electrolytes for application in the aqueous all copper redox flow battery, J. Power Sources 278 (2015) 175–182, https://doi.org/10.1016/j.jpowsour.2014.12.034.
[17] L. Sanz, D. Lloyd, E. Magdalena, J. Palma, K. Kontturi, Description and performance of a novel aqueous all-copper redox flow battery, J. Power Sources 268 (2014) 121–128, https://doi.org/10.1016/j.jpowsour.2014.06.008.
[18] P. Leung, J. Palma, E. Garcia-Quismondo, L. Sanz, M.R. Mohamed, M. Anderson, Evaluation of electrode materials for all-copper hybrid flow batteries, J. Power Sources 310 (2016) 1–11, https://doi.org/10.1016/j.jpowsour.2015.12.069.
[19] E.A. Stricker, K.W. Krueger, R.F. Savinell, J.S. Wainright, Investigating a bromide supported electrolyte for an all-copper flow battery, J. Electrochem. Soc. 165 (2018) A1797–A1804, https://doi.org/10.1149/2.1031809jes.
[20] M. Lundström, J. Aromaa, O. Forsén, Redox potential characteristics of cupric chloride solutions, Hydrometallurgy 95 (2009) 285–289, https://doi.org/10.1016/j.hydromet.2008.06.009.
[21] N.C. Hoyt, K.L. Hawthorne, R.F. Savinell, J.S. Wainright, Plating utilization of carbon felt in a hybrid flow battery, J. Electrochem. Soc. 163 (1) (2016) A5041–A5048, https://doi.org/10.1149/2.0061601jes.
[22] R.K. Gautam, M. Kapoor, A. Verma, Tactical surface modification of a 3D graphite felt as an electrode of vanadium redox flow batteries with enhanced electrolyte utilization and fast reaction kinetics, Energy Fuels 34 (2020) 5060–5071, https://doi.org/10.1021/acs.energyfuels.0c00701.
[23] X. Zhou, X. Zhang, L. Mo, X. Zhou, Q. Wu, Densely populated bismuth nanosphere semi-embedded carbon felt for ultrahigh-rate and stable vanadium redox flow batteries, Small 16 (2020) 1907333, https://doi.org/10.1002/smll.201907333.
[24] Q. Wu, X. Zhang, Y. Lv, L. Lin, Y. Liu, X. Zhou, Bio-inspired multiscale-pore-network structured carbon felt with enhanced mass transfer and activity for vanadium redox flow batteries, J. Mater. Chem. A 6 (2018) 20347–20355, https://doi.org/10.1039/C8TA06445H.
[25] X. Zhou, X. Zhang, Y. Lv, L. Lin, Q. Wu, Nano-catalytic layer engraved carbon felt via copper oxide etching for vanadium redox flow batteries, Carbon 153 (2019) 674–681, https://doi.org/10.1016/j.carbon.2019.07.072.
[26] W. Zhang, J. Xi, Z. Li, H. Zhou, L. Liu, Z. Wu, X. Qiu, Electrochemical activation of graphite felt electrode for VO^{2+}/VO_2^+ redox couple application, Electrochim. Acta 89 (2013) 429–435, https://doi.org/10.1016/j.electacta.2012.11.072.
[27] L. Eifert, R. Banerjee, Z. Jusys, R. Zeis, Characterization of carbon felt electrodes for vanadium redox flow batteries: impact of treatment methods, J. Electrochem. Soc. 165 (2018) A2577–A2586, https://doi.org/10.1149/2.0531811jes.
[28] B. Sun, M. Syllas-Kazacos, Modification of graphite electrode materials for vanadium redox flow battery application-1. Thermal treatment, Electrochim. Acta 37 (1992) 1253–1260, https://doi.org/10.1016/0013-4686(92)85064-R.
[29] S. Zhong, C. Padeste, M. Kazacos, M. Skyllas-Kazacos, Comparison of the physical, chemical and electrochemical properties of rayon- and polyacrylonitrile-based graphite felt electrodes, J. Power Sources 45 (1993) 29–41, https://doi.org/10.1016/0378-7753(93)80006-B.
[30] L.F. Castañeda, F.C. Walsh, J.L. Nava, C. Ponce de Leon, Graphite felt as a versatile electrode material: properties, reaction environment, performance and applications, Electrochim. Acta 258 (2017) 1115–1139, https://doi.org/10.1016/j.electacta.2017.11.165.
[31] D.A. Shirley, High-resolution X-ray photoemission spectrum of the valence bands of gold, Phys. Rev. B 5 (1972) 4709–4714. https://journals.aps.org/prb/pdf/10.1103/PhysRevB.5.4709.
[32] V. Di Noto, E. Negro, S. Polizzi, P. Riello, P. Atanassov, Preparation, characterization and single-cell performance of a new class of Pd-carbon nitride electrocatalysts for oxygen reduction reaction in PEMFCs, Appl. Catal. B Environ. 111–112 (2012) 185–199, https://doi.org/10.1016/j.apcatb.2011.09.034.
[33] G. Daniel, Y. Zhang, S. Lanzalaco, F. Brombin, T. Kosmala, G. Granozzi, A. Wang, E. Brillas, I. Sirés, C. Durante, Chitosan-derived nitrogen-doped carbon electrocatalyst for a sustainable upgrade of oxygen reduction to hydrogen peroxide in UV-assisted electro-fenton water treatment, ACS Sustain. Chem. Eng. 8 (2020) 14425–14440, https://doi.org/10.1021/acssuschemeng.0c04294.
[34] M. Angelo do Amaral Junior, J.T. Matsushima, M.C. Rezende, E.S. Gonçalves, J. Saldanha Marcuzzo, M.R. Baldan, Production and characterization of activated carbon fiber from textile PAN fiber, J. Aero. Technol. Manag. 9 (4) (2017) 423, https://doi.org/10.5028/jatm.v9i4.831.
[35] A. Sadezky, H. Muckenhuber, H. Grothe, R. Niessner, U. Pöschl, Raman microspectroscopy of soot and related carbonaceous materials: spectral analysis and structural information, Carbon 43 (2005) 1731–1742, https://doi.org/10.1016/j.carbon.2005.02.018.
[36] R. Banerjee, N. Bevilacqua, A. Mohseninia, B. Wiedemann, F. Wilhelm, J. Scholta, R. Zeis, Carbon felt electrodes for redox flow battery: impact of compression on transport properties, J. Energy Storage 26 (2019) 100997, https://doi.org/10.1016/j.est.2019.100997.
[37] J. Gonzàlez-Garcìa, P. Bonete, E. Expòsito, V. Montiel, A. Aldaza, R. Torregrosa-Macià, Characterization of a carbon felt electrode: structural and physical properties, J. Mater. Chem. 9 (1999) 419–426, https://doi.org/10.1039/A805823G.
[38] A.E. Rue1, M.M. Collinson, Size and shape control of gold nanodeposits in an array of silica nanowells on a gold electrode, Int. J. Electrochem. (2012), https://doi.org/10.1155/2012/971736, 971736.
[39] Y. Meng, A.J. Bard, Measurement of temperature-dependent stability constants of Cu(I) and Cu(II) chloride complexes by voltammetry at a Pt ultramicroelectrode, Anal. Chem. 87 (2015) 3498–3504, https://doi.org/10.1021/acs.analchem.5b00052.
[40] G. Lacarbonara, L. Faggiano, S. Porcu, P.C. Ricci, S. Rapino, D.P. Casey, J.F. Rohan, C. Arbizzani, Copper chloro-complexes concentrated solutions: an electrochemical study, Batteries 7 (2021) 83, https://doi.org/10.3390/batteries7040083.